Induction of a transmissible tau pathology by traumatic brain injury

Elisa R. Zanier[1]*, Ilaria Bertani[2], Eliana Sammali[1,3], Francesca Pischiutta[1], Maria Antonietta Chiaravalloti[2], Gloria Vegliante[1], Antonio Masone[2], Alessandro Corbelli[4], Douglas H. Smith[5], David K. Menon[6,7,8], Nino Stocchetti[9,10], Fabio Fiordaliso[4], Maria-Grazia De Simoni[11], William Stewart[12,13], Roberto Chiesa[2]*

[1]Laboratory of Acute Brain Injury and Therapeutic Strategies, Department of Neuroscience, IRCCS – Istituto di Ricerche Farmacologiche Mario Negri, Via G. La Masa 19, 20156 Milan, Italy

[2]Laboratory of Prion Neurobiology, Department of Neuroscience, IRCCS – Istituto di Ricerche Farmacologiche Mario Negri, Via G. La Masa 19, 20156 Milan, Italy

[3]Department of Cerebrovascular Diseases, Fondazione IRCCS – Istituto Neurologico Carlo Besta, Milan, Italy

[4]Bio-Imaging Unit, Department of Cardiovascular Research, IRCCS – Istituto di Ricerche Farmacologiche Mario Negri, Via G. La Masa 19, 20156 Milan, Italy

[5]Penn Centre for Brain Injury and Repair and Department of Neurosurgery, Perelman School of Medicine, University of Pennsylvania, Philadelphia, PA 19104, USA

[6]John van Geest Centre for Brain Repair, University of Cambridge, Cambridge CB2 0QQ, UK

[7]Division of Anaesthesia, Department of Medicine, University of Cambridge, Cambridge CB20QQ, UK

[8]Wolfson Brain Imaging Centre, Department of Clinical Neurosciences, University of Cambridge, Cambridge, CB2 0QQ, UK

[9]Department of Pathophysiology and Transplants, University of Milan, 20122 Milan, Italy

[10]Fondazione IRCCS Cà Granda Ospedale Maggiore Policlinico di Milan, 20122 Milan, Italy

[11]Laboratory of Inflammation and Nervous System Diseases, Department of Neuroscience, IRCCS – Istituto di Ricerche Farmacologiche Mario Negri, Via G. La Masa 19, 20156 Milan, Italy

[12]Institute of Neuroscience and Psychology, University of Glasgow, Glasgow G12 8QQ, UK

[13]Department of Neuropathology, Queen Elizabeth University Hospital, Glasgow G51 4TF, UK

Correspondence should be addressed to E.R.Z. (elisa.zanier@marionegri.it, phone: +39-02-39014204) or R.C. (roberto.chiesa@marionegri.it, phone: +39-02-39014428).

Running title: Brain trauma induces tau prion

Abstract

Traumatic brain injury is a risk factor for subsequent neurodegenerative disease, including chronic traumatic encephalopathy, a tauopathy mostly associated with repetitive concussion and blast, but not well recognized as a consequence of severe traumatic brain injury. Here we show that a single severe brain trauma is associated with the emergence of widespread hyperphosphorylated tau pathology in a proportion of humans surviving late after injury. In parallel experimental studies, in a model of severe traumatic brain injury in wild-type mice, we found progressive and widespread tau pathology, replicating the findings in humans. Brain homogenates from these mice, when inoculated into the hippocampus and overlying cerebral cortex of naive mice, induced widespread tau pathology, synaptic loss, and persistent memory deficits. These data provide evidence that experimental brain trauma induces a self-propagating tau pathology, which can be transmitted between mice, and call for future studies aimed at investigating the potential transmissibility of trauma associated tau pathology in humans.

Keywords

Traumatic brain injury, tau pathology, prion, neurological dysfunction, neurodegeneration

Introduction

Traumatic brain injury (TBI) is a recognized risk factor for delayed neurodegeneration and dementia, particularly chronic traumatic encephalopathy (CTE). The neuropathological picture that is emerging with late survival from TBI is of a complex of pathologies featuring abnormalities in tau, amyloid beta, neuronal loss, axonal degeneration, neuroinflammation and blood-brain barrier disruption (Johnson *et al.*, 2012, 2013; Hay *et al.*, 2016). Of particular note is the emergence of hyperphosphorylated forms of the microtubule-associated protein tau in a stereotypical pattern and distribution regarded as pathognomonic of CTE (McKee *et al.*, 2016). Specifically, in its early stage, CTE is recognized through the demonstration of clusters of perivascular neurons and glia containing hyperphosphorylated tau (P-tau), typically with patchy distribution and concentrated towards the depths of cortical sulci (Geddes *et al.*, 1999; McKee *et al.*, 2014, 2016; Mez *et al.*, 2017). There is a suggestion of hierarchical progression of pathology from these initially focal and patchy cortical P-tau deposits to more widespread cortical, medial temporal and subcortical grey matter in late-stage disease (McKee *et al.*, 2014). However, the mechanisms by which this initially localized cortical pathology progresses to more widespread and generalized disease are still not known.

In Alzheimer's disease (AD), tau pathology appears to progress along neural networks, suggesting transcellular spread of tau through neural connections (Goedert *et al.*, 2016). *In vivo* studies have described the spreading of AD-related tau pathology from local sites to distant regions of the brain (Clavaguera *et al.*, 2009, 2013; de Calignon *et al.*, 2012; Ahmed *et al.*, 2014; Guo *et al.*, 2016), and it has been suggested that tau aggregates – or seeds – serve as the agent of this spread, transmitting the aggregated/hyperphosphorylated state from cell to cell in a prion-like fashion (Prusiner, 2012; Clavaguera *et al.*, 2013; Iba *et al.*, 2013, 2015; Woerman *et al.*, 2016). Prions are proteinaceous infectious agents consisting of misfolded prion protein (PrP^{Sc}), which propagate by imposing their abnormal structures on host-encoded cellular prion protein (PrP^{C}) (Prusiner, 1982). As PrP^{Sc} prions colonize the affected patient, they perturb the function of the nervous system, leading to motor and neurophysiological deficits, cognitive decline, and ultimately death (Chiesa, 2015). Whether TBI generates misfolded or aggregated forms of tau protein that propagate by inducing misfolding of native tau in injured tissue and can be transmitted from one individual to another (tau prions), is not clear (Prusiner, 2012; Mudher *et al.*, 2017). We hypothesized that late

P-tau deposition after severe TBI (sTBI) would show prion behaviour, and addressed this hypothesis in sequential steps. First, we set out to demonstrate and characterize the deposition of P-tau late after sTBI as distinct from P-tau deposition in 'normal' aged human controls. Second, we sought the emergence of self-propagating P-tau pathology in wild-type (WT) mice subjected to sTBI that replicated P-tau pathology observed in humans long after a single focal TBI. Finally, we went on to establish whether this TBI-induced tauopathy could be transmitted between mice and cause neurological deficits, satisfying the requirements for a *bona fide* tau prion.

Materials and methods

Study design. The aim of the study was to test whether a single severe focal TBI was able to induce a self-propagating tauopathy. First, we analyzed the deposition of P-tau late after single TBI in humans. Next, we characterized the temporal evolution of tau pathology in WT mice subjected to severe controlled cortical impact. Last, we tested whether authentic tau prions are generated after trauma by attempting the transmission of tauopathy to naive mice by intracerebral inoculation of brain homogenates from TBI mice.

Male C57BL/6J mice (8 to 9 weeks of age) from Envigo were used in this study. The animals were housed four per cage at controlled temperature (22 ± 2°C) and relative humidity (60 ± 5%) with a 12/12-hour light/dark cycle and free access to pelleted food and water.

All animal experiments were designed in accordance with the ARRIVE (Animal Research: Reporting of In Vivo Experiments) guidelines (Kilkenny *et al.*, 2010), with a commitment to refinement, reduction, and replacement, minimizing the numbers of mice, while using biostatistics to optimize mouse numbers (as in our previously published peer-reviewed work using the mouse TBI model (Zanier *et al.*, 2016) and prion inoculation in mice (Bouybayoune *et al.*, 2015)). Thus, for statistical validity, we used 8 to 12 for the behavioural tests, and 3 to 8 for biochemical analysis and histology. The mice were assigned to the different experimental groups using randomization lists (www.randomizer.org). Inoculations, behavioural and histological assessments were done by researchers blinded to the experimental groups.

Ethics statement. Human tissue was obtained from the Glasgow TBI Archive of the Department of Neuropathology, Queen Elizabeth University Hospital, Glasgow, UK. Tissue samples were

acquired at routine diagnostic autopsy, with approval from the Greater Glasgow and Clyde Biorepository Governance Committee for their use in research. Procedures involving animals and their care were conducted in conformity with the institutional guidelines at the IRCCS – Mario Negri Institute for Pharmacological Research in compliance with national (D.lgs 26/2014; Authorization n. 19/2008-A issued March 6, 2008 by Ministry of Health) and international laws and policies (EEC Council Directive 2010/63/UE; the NIH Guide for the Care and Use of Laboratory Animals, 2011 edition). They were reviewed and approved by the Mario Negri Institute Animal Care and Use Committee that includes ad hoc members for ethical issues, and by the Italian Ministry of Health (Decreto no. D/07/2013-B and 301/2017-PR). Animal facilities meet international standards and are regularly checked by a certified veterinarian who is responsible for health monitoring, animal welfare supervision, experimental protocols and review of procedures.

Human studies. At the time of the original diagnostic autopsy, whole brains were immersion-fixed in 10% formal saline for a minimum of three weeks, then the specimens were examined, sampled and processed to paraffin tissue blocks. For this study, 15 patients surviving a year or more from single moderate or severe, closed TBI (defined as Glasgow Coma Scale at presentation < 13) and 15 age matched controls with no history of TBI or of known neurological disease were randomly selected from the comprehensive databases of the Glasgow TBI Archive by a laboratory research assistant with no knowledge of study purpose or design or of the pathologies in each of the TBI cases and controls selected. Full demographic information for late TBI cases and controls is contained in Supplementary Table 1. Information on TBI and controls history was obtained from review of diagnostic post-mortem and/or forensic reports. The TBI survival cases and the age-matched controls, had no recorded history of exposure to contact sports or military service, nor abuse or other injuries. Mechanism of injury is summarized in Supplementary Table 1. None were penetrating. From review of the original hospital records, at presentation, intracerebral haemorrhage was present in 5 cases, subdural a further 7, with 3 cases having no evidence of intracranial haemorrhage. Following the original TBI, all cases were discharged from hospitalization following recovery and, ultimately, died from causes of death unrelated to TBI. None were in a persistent vegetative state prior to death. Each case was sampled and assessed for this study as standardized regions, no matter the injury severity or location. As this study accesses archival tissue blocks, there were necessary restrictions on availability of sampled regions. Nevertheless, the standardized sampling protocols employed at the original diagnostic autopsy

included a coronal slice of the cerebral hemispheres at mid-thalamic level from which tissue blocks from multiple brain regions were selected for the purposes of this study to include: the corpus callosum with adjacent cingulate gyrus; the medial temporal lobe to include the hippocampus and entorhinal cortex; the insular cortex and the thalamus. From these tissue blocks 8 μm sections were prepared for immunohistochemistry procedures. After deparaffinization and rehydration, endogenous peroxidase was quenched by immerging sections in 3% aqueous H_2O_2 for 15 minutes. Then, heat-induced antigen retrieval was done using a microwave pressure cooker for 8 minutes in preheated 0.1 M Tris EDTA buffer (pH 8), followed by blocking in 50 mL of normal horse serum (Vector Labs, Burlingame, CA, USA) per 5 mL of Optimax buffer (BioGenex, San Ramon, CA, USA) for 30 minutes. The sections were then incubated in antibody to phosphorylated tau (PHF1; 1:1000; gift from P. Davies, Feinstein Institute for Medical Research, Manhasset, NY, USA) at 4°C for 20h prior to washing and application of biotinylated secondary antibody for 30 minutes, followed by an avidin biotin complex, as per the manufacturer's instructions (Vectastain Universal Elite Kit, Vector Labs, Burlingame, CA, USA). The target antigen was visualized using the DAB peroxidase substrate kit (Vector Labs, Burlingame, CA, USA), with the sections then counterstained with hematoxylin. Control sections (positive and negative) for each antibody were run in parallel with the test sections to confirm antibody specificity. Sections were viewed blind to whether they were TBI or control, using a Leica DMRB light microscope (Leica Microsystems, Wetzlar, Germany) and the extent and distribution of tau pathology was assessed and semi-quantitatively scored as: Score 0, where no tau pathology was present; Score 1, PHF1 pathology comprising immunoreactive NFT and neurites of sparse to moderate density in the transentorhinal cortex with or without small numbers in the CA1 sector of the hippocampus; Score 2, PHF1-immunoreactive NFT and neurites as described for Score 1 together with NFTs extending into the fusiform gyrus (lateral to entorhinal cortex) and sparse tangles in the cortex (cingulate/insular blocks); Score 3, contained PHF1-immunoreactive NFT and neurites in more widespread sectors of the hippocampus and subiculum, with extensive medial temporal, cingulate and insular cortical involvement.

Mouse model of traumatic brain injury. The controlled cortical impact brain injury mouse model used in this study accurately replicates both the mechanical forces and the main secondary injury processes observed in severe TBI patients with brain contusion and is associated with clinically-relevant behavioural and histopathological outcomes (Smith *et al.*, 1995; Pischiutta *et*

al., 2018). Mice were anesthetized by isoflurane inhalation (induction 3%; maintenance 1.5%) in an N_2O/O_2 (70%/30%) mixture and placed in a stereotaxic frame. Rectal temperature was maintained at 37°C. Mice were then subjected to craniectomy followed by induction of controlled cortical impact brain injury as previously described (Zanier *et al.*, 2016). Briefly, the injury was induced using a 3-mm rigid impactor driven by a pneumatic piston rigidly mounted at an angle of 20° from the vertical plane and applied to the exposed dura mater, between bregma and lambda, over the left parieto-temporal cortex (antero-posteriority: –2.5 mm, laterality: –2.5 mm), at an impactor velocity of 5 m/s and deformation depth 1 mm, resulting in a severe level of injury (Smith *et al.*, 1995). The craniotomy was then covered with a cranioplasty and the scalp sutured. Sham mice received identical anesthesia and surgery without brain injury.

Transmission Studies. Brain homogenates (10% w/v in PBS) from the ipsi and contralateral cerebral cortex (including all the cortical tissue above the rhinal fissure) of mice 12 months from TBI or sham injury were inoculated in the hippocampus (A/P, –2.5 mm from bregma; L, ±2.0 mm; D/V, –1.8 mm) and overlaying cerebral cortex (A/P, –2.5 mm from bregma; L, ±2.0 mm; D/V, –0.8 mm). Inocula were from single brains. The TBI brain homogenates showing the highest amounts of P-tau by Western blot were chosen for inoculation. Mice were injected bilaterally (2.5 µL each, injection speed of 1.25 µL/min).

Novel object recognition. Mice were tested in an open-square grey arena (40 x 40 cm), 30 cm high, with the floor divided into 25 squares by black lines. The following objects were used: a black plastic cylinder (4 x 5 cm), a glass vial with a white cap (3 x 6 cm) and a metal cube (3 x 5 cm). The task started with a habituation trial during which mice were placed in the empty arena for 5 minutes and their movements were recorded as the number of line-crossings. The next day, mice were placed in the same arena containing two identical objects (familiarization phase). Exploration was recorded in a 10-minute trial by an investigator blinded to the experimental group. Sniffing, touching and stretching the head toward the object at a distance of no more than 2 cm were scored as object investigation. Twenty-four h later (test phase) mice were placed in the arena containing two objects: one identical to one of the objects presented during the familiarization phase (familiar object), and a new, different one (novel object), and the time spent exploring the two objects was recorded for 10 min. Memory was expressed as a discrimination index, i.e. the time spent exploring the novel object minus the time spent exploring the familiar one, divided by

the total time spent exploring both objects; the higher the discrimination index, the better the performance.

Immunohistochemistry and immunofluorescence. Mice were euthanized by cervical dislocation, brains were removed and fixed in 10% formalin for 24h, dehydrated in graded ethanol solutions, cleared in xylene, and embedded in paraffin. Serial sections (5 μm thick) were cut onto glass slides and boiled in citrate buffer (10 mM pH 6.0, Dako) for antigen retrieval, followed by incubation with the following anti-tau monoclonal antibodies: AT8 (phospho-tau Ser202/Thr205; Thermo Fisher; 1:1000), AT180 (phospho-tau Thr231; Thermo Fisher; 1:1000), PHF1 (Ser396/Ser404; from P. Davies; 1:4000) and MC1 (aa 312-322; from P. Davies; 1:100). AT8 and AT180 immunostaining was visualized using the ARK kit (Dako). For secondary staining of MC1 and PHF1, slices were incubated with biotinylated goat anti-mouse IgG1 in Superblock Solution (Pierce), followed by visualization with the TSA Biotin System (Perkin Elmer) and DAB (diaminobenzidine) Substrate Chromogen System (Dako).

Slices were examined by an Olympus BX-61 Virtual Stage microscope, interfaced with VS-ASW-FL software (Olympus Tokyo, Japan). For quantification of the AT8-positive staining in TBI mice regions of interest (ROI) were selected according to the Paxinos atlas (Paxinos and Franklin, 2004) in coronal (bregma -1.6 mm) and sagittal (lateral 1.5 mm) sections. In TBI mice the ipsilateral cortex was analysed over an area 1 mm deep from the edge of the contusion (Pischiutta *et al.*, 2018) and the contralateral from midline to the entorinal cortex. In the inoculated mice ROIs included whole cortex, hippocampus, thalamus and cerebellum. The same ROIs were selected in sham mice. Images were acquired using a 60X oil objective with pixel size 0.115 μm. Acquisition was done over 5 μm thick stacks, with step size 1 μm. The different focal planes were merged into a single stack by mean intensity projection to ensure consistent focus throughout the sample. Images were analysed using Fiji software (http://fiji.sc/Fiji).

The digital separation of DAB staining from hematoxylin signal was done by color deconvolution (http://www.mecourse.com/landinig/software/cdeconv/cdeconv.html) and the DAB channel was used for quantification. To ensure consistency of the segmentation in the image processing, we subtracted the intensity background from the image calculated by averaging non-specific signal in identified region of interest. Specific signal after the image processing was computed as positive pixels/total pixels, and reported as the percentage stained area for statistical analysis.

For immunofluorescence, brain sections on glass slides were boiled in citrate buffer and incubated in blocking solution with the following primary antibodies: anti-drebrin (Fitzgherald, 1:200) an actin-binding protein enriched in dendritic spines, (Sekino *et al.*, 2017) and anti-vesicular glutamate transporter-1 (VGLUT-1, Synaptic System, 1:6000), for analysis of the presynaptic compartment (Senatore *et al.*, 2012). Slices were then incubated with biotinylated secondary antibody (Vecstain, 1:500) and streptavidin 647 (Molecular Probes, 1:500), and examined by confocal microscopy (FV-500 Olympus) acquiring images in two different areas of CA1 field of the hippocampus using a 60X oil objective. Z-Stack images were acquired: 0.2 µm z-distance, 3 µm thick confocal z-stacks (optical section depth 0.2 µm, 21 sections/z-stack) and 1024x1024 pixel resolution. Confocal Images were deconvoluted (CellP) and puncta were identified with Imaris software using the "quality" parameter (Heise *et al.*, 2016). Only puncta stringently conforming with the quality parameter entered analysis.

Biochemical analysis. Frozen brain tissue was homogenized in 10 volumes of PBS. Homogenates were aliquoted and stored at -80°C until use. Western blot analysis of total brain homogenates with monoclonal antibody AT8 was done on heat-stable protein fractions prepared according to Petry et al. (Petry *et al.*, 2014) to avoid the interfering signal due to endogenous immunoglobulins. Proteins (50 µg) were separated on Nu-Page 4-12% gels (Thermo Scientific) and blotted onto nitrocellulose membranes (Hybond, GE Healthcare). After blocking with 5% dry milk for 1h at room temperature, membranes were incubated overnight at 4°C with anti-total Tau (1:10000, Dako) or AT8 (1:500, Thermo Scientific), then with HRP-conjugated secondary antibodies (Santa Cruz). Peroxidase activity was detected using an ECL (Iluminata Forte) kit (Millipore, Billerica, MA, USA) and visualized with a ChemiDoc imaging system (Bio-Rad). For RIPA insoluble preparation 100 µL of brain homogenate were incubated for 20 min on an orbital shaker with 1% RIPA buffer (50 mM Tris-HCl, pH 7.4, 1% NP-40, 150 mM NaCl, 0.25% Na-deoxycholate, 1 mM EDTA, 1 mM Na_3VO_4, 1 mM NaF, 1 mM PMSF and protease inhibitors). Brain extract was ultracentrifuged for 60 min at 100000 g at room temperature. The pellet was resuspended in 450 µL of RIPA buffer and ultracentrifuged at 100000 g for 30 min at room temperature. The supernatant was carefully removed and the pellet was resuspended in 100 µL of 1X Laemmli sample buffer and proteins analyzed by Western blot.

For assay of protease resistance brain lysates prepared in 0.05% Triton X-100 in PBS were centrifuged at 300 g for 5 min. Proteins (20 µg) in the supernatants were digested with pronase (0-10 µg/mL; Sigma) in a final volume of 20 µL for 1 h at 37°C, then resolved by Nu-Page 4-12% gels and analysed by Western blot with primary anti-tau antibody BR135 (1:1000, gift from M. Goedert, MRC Laboratory of Molecular Biology, Cambridge, UK (Goedert *et al.*, 1989)).

Electron microscopy. Three controls and three TBI inoculated mice were deeply anesthetized and perfused through the ascending aorta with phosphate buffered saline (PBS, 0.1 M; pH 7.4) followed by a 5 minute perfusion with 4% paraformaldehyde. Hippocampus was excised and cut in sagittal plane with a razor blade and postfixed in 4% paraformaldehyde and 2% glutaraldehyde in phosphate buffer 0.12 M, then for 2h in OsO4. After dehydration in graded series of ethanol, tissue samples were cleared in propylene oxide, embedded in Epoxy medium (Epoxy Embedding Medium kit; Sigma-Aldrich) and polymerized at 60°C for 72h. From each sample, one semithin (1 µm) section was cut with a Leica EM UC6 ultramicrotome and mounted on glass slides for light microscopic inspection to identify the stratum oriens of the hippocampus. Ultrathin (70 nm thick) sections of the areas of interest were obtained, counterstained with uranyl acetate and lead citrate, and examined with an Energy Filter Transmission Electron Microscope (Libra120, Carl Zeiss NTS GmbH) equipped with a yttrium aluminium garnet scintillator slow-scan charge-coupled device camera (Sharp eye, TRS, Moorenweis, Germany). A ROI including the postsynaptic density (PSD) was manually traced and its area and thickness measured by iTem software (Olympus Soft Imaging Solutions, Germany) of 263 synapses in control inoculated mice and 262 in TBI inoculated mice fitting the following two criteria: (1) presence of a cluster of presynaptic vesicles (at least 3 of them); (2) presence of a defined synaptic cleft.

Statistical analysis. All graphs represent the mean ± SEM. GraphPad Prism 7 was used for statistical analyses. A categorical assessment score was used to assess human tau deposition. Results were dichotomized in either ‘low’ score (0-1) or ‘high’ score (2-3) and the Chi square test was used to assess differences between groups. Data in mice were analysed by one-way analysis of variance (ANOVA), followed by Tukey’s test to assess differences in case of three or more groups (behavioural tests and temporal changes of tau deposition) or by unpaired t test. P values < 0.05 were considered to be statistically significant.

Results

Late P-tau deposition is common in human survivors of a single moderate/severe TBI, and exceeds that seen in age-matched controls.

Representative tissue sections from the brains of patients surviving a median of 5 years (range: 1-18 years) following a single moderate or severe, closed TBI [n=15; age 19-89 (median 60) years], or control subjects with no history of TBI or known neurological disease [n=15; age 20-92 (median 60) years] (Supplementary Table 1) were stained for P-tau using antibody PHF1. In TBI patients surviving a year or more, PHF1-immunreactive profiles appeared as neurofibrillary tangles and immunoreactive neurites (singly and in plaques), astrocytes and plaques within all cortical layers, although often with higher density in the superficial cortical layers (Fig. 1A). Elsewhere, where hippocampal profiles were present, all sectors appeared involved, CA2 less frequent than other sectors in this series. Six cases showed involvement of structures in the region of the thalamus as sparse immunoreactive thalamic or nigral neurons, occasional neurites and immunoreactive astrocytes. Although the proportions of patients with PHF1-immunoractive tau pathology were similar in controls and TBI (12 cases with pathology in each group), the extent and distribution of the pathologies were considerably greater in survivors of TBI than in non-injured controls (Fig. 1B). Specifically, in controls, PHF1-immunoreactive NFTs and neurites were largely restricted to sparse profiles in the entorhinal cortex, with just four cases showing more extensive pathologies extending to the hippocampus and cortex. In contrast, in late survivors of TBI, 9 of 12 PHF1-immunoreactive cases displayed higher stage tau pathology, with PHF1-immunoreactive profiles in moderate to high density across the medial temporal lobe, including the hippocampus, and extending to the cortex. Neuritic P-tau positive profiles were found in the neuropil, many with a truncated, granular appearance as illustrated in Fig 1A. In three of 12 TBI cases with P-tau pathology immunoreactive neuronal and glial profiles showed focal clustering around cortical vessels, in two of these at the depths of sulci (Fig. 1A); appearances consistent with the pathognomonic pathology of CTE described in the preliminary NIH diagnostic criteria (McKee *et al.*, 2016). One further TBI case, an 87 year old male with a 5 year survival following a road traffic accident, showed clusters of P-tau immunoreactive subpial astrocytes in the medial temporal lobe, consistent with ageing related tau astrogliopathy (Kovacs *et al.*, 2016). Both in late TBI cases and controls the extent of P-tau pathology appeared to increase with increasing age; the higher score pathology encountered more often with increasing age. Specifically, the 4 controls with higher tau

scores (2 or 3) were among the older aged (74 years or above) controls. Of note, while again typically older within the cohort, the 9 late TBI cases with higher tau scores ranged from a younger age (age 59 years upwards) than controls. No clear association between survival duration and extent of tau pathology could be ascertained in this small series (Supplementary Fig. 1). In keeping with injury severity, evidence of healed contusion was near ubiquitous; present in all but 1 case. There was no association between presence or nature of intracranial haemorrhage, including contusions, and tau pathology.

Single severe TBI induces a progressive tau pathology that spreads from the site of injury to remote brain regions in WT mice.

We tested whether single focal brain trauma triggered propagating tau pathology in WT mice. Two-month-old C57BL/6J mice were subjected to sTBI (16 mice) or to sham injury (14 mice). Eight TBI and seven sham were sacrificed at 3 months and used for immunohistochemistry (IHC; 4 TBI and 4 sham) or biochemical analysis (4 TBI and 3 sham). One TBI mouse was found dead at about four months, and the brain was not collected due to prolonged post-mortem delay. The remaining mice were culled at 12 months and used for IHC (4 TBI and 5 sham) and for biochemistry (3 TBI and 2 sham).

Phospho-tau immunopositivity, assessed by AT8, AT180 and PHF1 antibodies, was evident in two out of four mice at 3 months post TBI and restricted to the hemisphere ipsilateral to injury, with concentration to the regions adjacent to injury (Fig. 2A, compare panels i and ii, and Fig. 2B, and Supplementary Fig. 2). In contrast at 12 months, both ipsi- and contralateral P-tau pathologies were present, supporting progressive spreading of tau pathology from the injured hemisphere (Fig. 2A, compare panels i and iii, and Fig. 2B, Fig. 2C, compare panels iv and vi, and Fig. 2D, and Supplementary Fig. 2). Western blot analysis found increased levels of total and AT8-reactive tau in 1 frozen TBI brain compared to sham-injured controls at 3 months and in 2 out of 3 TBI brains at 12 months (and example is shown in Supplementary Fig. 3). Thus, 3 out of 7 TBI mice (~40%) developed pathological tau at 3 months, and 6 out of 7 (~85%) at 12 months.

P-tau was observed as neuronal cytoplasmic, neuritic and glial profiles throughout the cerebral cortex, hippocampus (CA1 and CA3 fields) and thalamus, with pathology also in the striatum and zona incerta (Fig. 3). In addition, a notable observation was numerous small to medium sized, rounded, ‘grain-like’ profiles, particularly within the neuropil (Fig. 3C). Occasionally there was

faint clustering of these granular immunoreactive profiles (Fig. 3G), with still other examples showing apparent localization along cortical vessels (Fig. 3H). Elsewhere, glial cytoplasmic P-tau immunoreactivity was present within white matter of the corpus callosum.

Tau prions are generated in TBI mice, causing transmission of tau pathology, synaptic loss and behavioural deficits.

The evidence that TBI induced a P-tau pathology that progressively spread throughout the brain suggested formation of a self-templating tau conformation. To test whether this could be horizontally transmitted like a prion, causing brain dysfunction, we intracerebrally inoculated 10% brain homogenates from TBI and sham-injured mice into naive C57BL/6J mice. Brain homogenates of contused and contralateral hemispheres (TBI_{ipsi} and TBI_{contra}, respectively) showing increased levels of total and AT8-positive tau by Western blot at 12 months post TBI (Supplementary Fig. 3) were inoculated bilaterally into the hippocampus and overlaying cerebral cortex of the recipient mice (Fig. 4A). The mice were examined in the novel object recognition (NOR) test 8 and 12 months post inoculation (m.p.i.). There was an overt memory deficit in the TBI_{ipsi}- but not in the TBI_{contra}-inoculated mice at 8 m.p.i. (Fig. 4B). At 12 m.p.i the memory deficit persisted in the TBI_{ipsi}- and was also detected in the TBI_{contra}-inoculated mice (Fig. 4C). No memory deficit was seen in mice inoculated with sham-injured brain tissue.

This was confirmed in an independent experiment in which we tested the effect of the inoculation of TBI brain homogenate, obtained from the injured hemisphere 12 months post injury, on recognition memory in the inoculated animals at an earlier time (4 m.p.i). Memory was already significantly impaired at four months, and this was confirmed at 8 m.p.i. (Fig. 5B and C). Locomotor activity was similar in sham and TBI inoculated mice, indicating that the deficit in the NOR test was not due to motor abnormalities (Fig. 4D and E, and Fig. 5D and E).

The memory deficit was associated with hippocampal synaptic pathology. Analysis of pre- and post-synaptic compartments by quantitative VGLUT-1 and drebrin immunofluorescence showed marked synaptic loss in the stratum oriens of the CA1 region at 12 m.p.i. (Fig. 6A and B). Electron microscopy examination showed a significant decrease in PSD thickness and area in hippocampal synapses in TBI inoculated mice (Fig. 6C) consistent with impaired synaptic efficacyAnalysis of P-tau deposition by antibody AT8 showed a significant difference between sham and TBI inoculated mice not only at the site of injection, but also widespread throughout the brain (Fig. 7).

Specifically, P-tau neurons, neurites and glia were identified in the cerebral cortex, hippocampus (CA1, CA3, and hilus of the dentate gyrus) and thalamus, with morphologies similar to those observed in mice exposed to TBI, including widespread 'grain-like' profiles (Fig. 8B-I). In the cerebellum, P-tau immunoreactive cytoplasmic and neuritic inclusions were noted in association with Purkinje cells and within the granule cell layer (Fig. 8J-K). Consistent with widespread tau pathology, there was an increase in the amount of aggregated tau in the thalamus of TBI-inoculated mice (Supplementary Fig. 4). The tau conformer that accumulated in the brains of TBI-inoculated mice was partially resistant to protease digestion, yielding a pronase-resistant fragment of ~10 kDa (Supplementary Fig. 4C), consistent with tau prion formation (Sanders *et al.*, 2014; Kaufman *et al.*, 2016).

Discussion

The present study found that a single moderate or severe TBI in humans resulted in widespread tau pathology with a notable pattern and distribution. Further, a single severe TBI induced persistent and evolving tau pathology in WT mice, with characteristics similar to late post TBI tau pathology in humans, which progressively spread from the site of injury to ipsi- and contralateral brain regions. This TBI generated tau pathology could be transmitted to WT recipient mice by intracerebral inoculation, inducing tau aggregation, memory deficits and synaptic alterations. These results indicate that tau prions are generated in TBI, providing a mechanistic explanation for how a biomechanical insult might trigger self-sustained neurodegeneration.

In the past decade, there has been growing recognition that repetitive mild TBI might set in motion brain pathological processes that place exposed individuals at risk for neurodegenerative disorders in mid-to-late life, particularly CTE. While there is also evidence that tau pathology may be seen many years after a single severe TBI, most attention has focused on the association between repeated mild TBI and CTE, with the common impression tau pathology is uniquely associated with repetitive mild TBI which dictates a distinct neurodegenerative disease.

Here we confirm that widespread CTE-like tau pathology is present in survivors of a year or more after just a single moderate to severe TBI in humans, and in mice exposed to sTBI surviving up to one year from injury. In our series of 15 patients who survived a year or more post TBI, we found 12 positive for tau. The extent and distribution of staining was considerably greater than that seen in age-matched, non-TBI controls, with some variation between TBI subjects. This inter-individual

variability appeared to follow a stereotypic pattern of deposition, reminiscent of hierarchical P-tau deposition in other neurodegenerative diseases (Braak and Braak, 1995; Kovacs, 2015). These data provide one possible neuropathological substrate for the increased or accelerated incidence of neurodegenerative disease in patients who survive a single moderate or severe TBI. Although the extent and distribution of P-tau pathology was greater in late TBI survivors, it was not possible to establish a clear association between survival interval and extent of tau pathology. Further, our data in this limited human study show similar percentages of cases with tau pathology in TBI and control groups, making it hard to establish whether TBI accelerates a preexisting age-related tauopathy, or triggers de novo tau deposition.

A better understanding of the biology that underlies this process calls for tractable experimental models. Previous investigations have shown that TBI accelerates genetically determined tau deposition in transgenic mice overexpressing mutant or WT human tau (Yoshiyama *et al.*, 2005; Hien T. Tran *et al.*, 2011; H. T. Tran *et al.*, 2011; Ojo *et al.*, 2016), and can lead to tauopathy in WT mice (Goldstein *et al.*, 2012; Kondo *et al.*, 2015; Meabon *et al.*, 2016). A few studies reported formation of tau aggregates shortly after sTBI in rats (Hawkins *et al.*, 2013; Gerson *et al.*, 2016), with only one study showing persistent tau pathology in WT mice (Kondo *et al.*, 2015). Our data not only confirm de novo tau deposition in WT animals after single TBI, but also document widespread tau immunopositivity at chronic stages, with a pattern echoing our observations in human TBI cases, including grain-like profiles in the neuropil and perivascular deposits. Interestingly we observed an increase in total tau after TBI. This could be due to increased tau expression or impaired tau clearance, perhaps because of TBI-induced alterations in proteostasis mechanisms, such as the glymphatic system (Iliff *et al.*, 2014), and/or formation of an intrinsically protease resistant tau conformer.

To establish a direct contribution of TBI induced tau pathology to late symptomatology in a clean setting, we performed inoculation studies in which there are no confounding factors inherent to the biomechanical injury. We found that inoculation of mouse TBI homogenates induced tau pathology with formation of partially protease resistant tau, memory deficits and synaptic alterations in WT recipient mice, providing evidence for generation of authentic tau prions. Previous studies showed that fibrillar forms of recombinant tau or tau aggregates from AD patients or other tauopathies can accelerate the genetically determined tau pathology in mutant tau cells and mice (Clavaguera *et al.*, 2009; Sanders *et al.*, 2014; Kaufman *et al.*, 2016; Woerman *et al.*,

2016). More recently, aggregated tau isolated from AD brains and other tauopathies was shown to induce tau pathology when inoculated intracerebrally in WT mice (Lasagna-Reeves *et al.*, 2012; Guo *et al.*, 2016; Narasimhan *et al.*, 2017), supporting the generation of self-propagating tau in AD. However, to the best of our knowledge no long-lasting memory deficits or other signs of brain dysfunction were documented in these animals, leaving open the question of whether toxic tau prions are formed in these models. The observation that TBI-induced tauopathy can be transmitted between WT mice and cause persistent memory deficits satisfies the main requirement for a toxic *bona fide* prion. Oligomeric or fibrillar forms of tau have been identified in different taupathies that may have distinct toxic potency and seeding properties (Goedert and Spillantini, 2017). Future studies should aim at identifying the abnormal tau species responsible for propagation of tau pathology and synaptic toxicity. It will also be important to immunodeplete tau from the inocula to rule out that persistent inflammatory processes and/or other TBI-related signalling pathways (Makinde *et al.*, 2017; Pischiutta *et al.*, 2018) may contribute to triggering tau pathology in the inoculated mice.

Host PrP^{C} is required for PrP^{Sc} replication and pathogenic effect (Chiesa, 2015). It will be interesting to assess if the same holds true for tau by testing the amnestic effect of TBI-induced tau prions in tau knockout mice. Finally, the development of bioassays and/or biochemical methods for measuring tau prion titers as for PrP^{Sc} prions, will enable to define the time lag between the biomechanical insult and the formation of the tau conformers responsible for seeding the spread of pathology. This will not only be important for therapeutic approaches targeting tau propagation (Holmes and Diamond, 2014), but also to assess the possible formation of infectious tau in humans post TBI. The demonstration of tau prions in human TBI will urgently require studies to determine whether neurosurgical intervention in such patients should conform to well established precautions for transmission of prion disease, as suggested by the Centers for Disease Control (https://www.cdc.gov/prions/cjd/infection-control.html) and the World Health Organization (http://www.who.int/csr/resources/publications/bse/WHO_CDS_CSR_APH_2000_3/en/).

Acknowledgments

We are grateful to Peter Davies for providing the PHF1 and MC1 antibodies and to Michael Goedert for the BR135 antibody. We also acknowledge Stefano Fumagalli and Pietro Veglianese for advice on quantification of immunofluorescent staining.

Funding

This work was supported by the National Institutes of Health (NIH NS094003 and NS038104) (DHS, WS); by NHS Research Scotland Career- Researcher Fellowship (WS); and the Alzheimer's Association (AARG-18-532633) (ERZ, RC); DKM was supported by a Senior Investigator award from the National Institute for Health Research (UK).

Bibliography

Ahmed Z, Cooper J, Murray TK, Garn K, McNaughton E, Clarke H, et al. A novel in vivo model of tau propagation with rapid and progressive neurofibrillary tangle pathology: the pattern of spread is determined by connectivity, not proximity. Acta Neuropathol 2014; 127: 667–83.

Bouybayoune I, Mantovani S, Del Gallo F, Bertani I, Restelli E, Comerio L, et al. Transgenic fatal familial insomnia mice indicate prion infectivity-independent mechanisms of pathogenesis and phenotypic expression of disease. PLoS Pathog 2015; 11: e1004796.

Braak H, Braak E. Staging of Alzheimer's disease-related neurofibrillary changes. Neurobiol. Aging 1995; 16: 271–278.

de Calignon A, Polydoro M, Suarez-Calvet M, William C, Adamowicz DH, Kopeikina KJ, et al. Propagation of tau pathology in a model of early Alzheimer's disease. Neuron 2012; 73: 685–97.

Chiesa R. The elusive role of the prion protein and the mechanism of toxicity in prion disease. PLoS Pathog 2015; 11: e1004745.

Clavaguera F, Akatsu H, Fraser G, Crowther RA, Frank S, Hench J, et al. Brain homogenates from human tauopathies induce tau inclusions in mouse brain. Proc. Natl. Acad. Sci. 2013; 110: 9535–9540.

Clavaguera F, Bolmont T, Crowther RA, Abramowski D, Frank S, Probst A, et al. Transmission and spreading of tauopathy in transgenic mouse brain. Nat Cell Biol 2009; 11: 909–13.

Geddes JF, Vowles GH, Nicoll JA, Révész T. Neuronal cytoskeletal changes are an early consequence of repetitive head injury. Acta Neuropathol. 1999; 98: 171–178.

Gerson J, Castillo-Carranza DL, Sengupta U, Bodani R, Prough DS, DeWitt DS, et al. Tau Oligomers Derived from Traumatic Brain Injury Cause Cognitive Impairment and Accelerate Onset of Pathology in Htau Mice. J. Neurotrauma 2016; 33: 2034–2043.

Goedert M, Masuda-Suzukake M, Falcon B. Like prions: the propagation of aggregated tau and alpha-synuclein in neurodegeneration [Internet]. Brain 2017; 140(2): 266-278.

Goedert M, Spillantini MG. Propagation of Tau aggregates. Mol. Brain 2017; 10(1): 18.

Goedert M, Spillantini MG, Jakes R, Rutherford D, Crowther RA. Multiple isoforms of human microtubule-associated protein tau: sequences and localization in neurofibrillary tangles of Alzheimer's disease. Neuron 1989; 3: 519–526.

Goldstein LE, Fisher AM, Tagge CA, Zhang XL, Velisek L, Sullivan JA, et al. Chronic traumatic encephalopathy in blast-exposed military veterans and a blast neurotrauma mouse model. Sci Transl Med 2012; 4: 134ra60.

Guo JL, Narasimhan S, Changolkar L, He Z, Stieber A, Zhang B, et al. Unique pathological tau conformers from Alzheimer's brains transmit tau pathology in nontransgenic mice. J. Exp. Med. 2016; 213: 2635–2654.

Hawkins BE, Krishnamurthy S, Castillo-Carranza DL, Sengupta U, Prough DS, Jackson GR, et al. Rapid accumulation of endogenous tau oligomers in a rat model of traumatic brain injury:

possible link between traumatic brain injury and sporadic tauopathies. J. Biol. Chem. 2013; 288: 17042–17050.

Hay J, Johnson VE, Smith DH, Stewart W. Chronic Traumatic Encephalopathy: The Neuropathological Legacy of Traumatic Brain Injury. Annu. Rev. Pathol. 2016; 11: 21–45.

Heise C, Schroeder JC, Schoen M, Halbedl S, Reim D, Woelfle S, et al. Selective Localization of Shanks to VGLUT1-Positive Excitatory Synapses in the Mouse Hippocampus. Front. Cell. Neurosci. 2016; 10: 106.

Holmes BB, Diamond MI. Prion-like properties of Tau protein: the importance of extracellular Tau as a therapeutic target. J Biol Chem 2014; 289: 19855–61.

Iba M, Guo JL, McBride JD, Zhang B, Trojanowski JQ, Lee VM-Y. Synthetic Tau Fibrils Mediate Transmission of Neurofibrillary Tangles in a Transgenic Mouse Model of Alzheimer's-like Tauopathy. J. Neurosci. 2013; 33: 1024–1037.

Iba M, McBride JD, Guo JL, Zhang B, Trojanowski JQ, Lee VM-Y. Tau pathology spread in PS19 tau transgenic mice following locus coeruleus (LC) injections of synthetic tau fibrils is determined by the LC's afferent and efferent connections. Acta Neuropathol. 2015; 130: 349–362.

Iliff JJ, Chen MJ, Plog BA, Zeppenfeld DM, Soltero M, Yang L, et al. Impairment of Glymphatic Pathway Function Promotes Tau Pathology after Traumatic Brain Injury. J. Neurosci. 2014; 34: 16180–16193.

Johnson VE, Stewart JE, Begbie FD, Trojanowski JQ, Smith DH, Stewart W. Inflammation and white matter degeneration persist for years after a single traumatic brain injury. Brain 2013; 136: 28–42.

Johnson VE, Stewart W, Smith DH. Widespread τ and amyloid-β pathology many years after a single traumatic brain injury in humans. Brain Pathol. 2012; 22: 142–149.

Kaufman SK, Sanders DW, Thomas TL, Ruchinskas AJ, Vaquer-Alicea J, Sharma AM, et al. Tau Prion Strains Dictate Patterns of Cell Pathology, Progression Rate, and Regional Vulnerability In Vivo. Neuron 2016; 92: 796–812.

Kilkenny C, Browne WJ, Cuthill IC, Emerson M, Altman DG. Improving bioscience research reporting: the ARRIVE guidelines for reporting animal research. PLoS Biol 2010; 8: e1000412.

Kondo A, Shahpasand K, Mannix R, Qiu J, Moncaster J, Chen CH, et al. Antibody against early driver of neurodegeneration cis P-tau blocks brain injury and tauopathy. Nature 2015; 523: 431–6.

Kovacs GG. Invited review: Neuropathology of tauopathies: principles and practice. Neuropathol. Appl. Neurobiol. 2015; 41: 3–23.

Kovacs GG, Ferrer I, Grinberg LT, Alafuzoff I, Attems J, Budka H, et al. Aging-related tau astrogliopathy (ARTAG): harmonized evaluation strategy. Acta Neuropathol. 2016; 131: 87–102.

Lasagna-Reeves CA, Castillo-Carranza DL, Sengupta U, Guerrero-Munoz MJ, Kiritoshi T, Neugebauer V, et al. Alzheimer brain-derived tau oligomers propagate pathology from endogenous tau. Sci Rep 2012; 2: 700.

Liu L, Drouet V, Wu JW, Witter MP, Small SA, Clelland C, et al. Trans-synaptic spread of tau pathology in vivo. PloS One 2012; 7: e31302.

Makinde HM, Just TB, Cuda CM, Perlman H, Schwulst SJ. The Role of Microglia in the Etiology and Evolution of Chronic Traumatic Encephalopathy. Shock 2017; 48: 276–283.

McKee AC, Cairns NJ, Dickson DW, Folkerth RD, Keene CD, Litvan I, et al. The first NINDS/NIBIB consensus meeting to define neuropathological criteria for the diagnosis of chronic traumatic encephalopathy. Acta Neuropathol. 2016; 131: 75–86.

McKee AC, Daneshvar DH, Alvarez VE, Stein TD. The neuropathology of sport. Acta Neuropathol. 2014; 127: 29–51.

Meabon JS, Huber BR, Cross DJ, Richards TL, Minoshima S, Pagulayan KF, et al. Repetitive blast exposure in mice and combat veterans causes persistent cerebellar dysfunction. Sci. Transl. Med. 2016; 8: 321ra6.

Mez J, Daneshvar DH, Kiernan PT, Abdolmohammadi B, Alvarez VE, Huber BR, et al. Clinicopathological Evaluation of Chronic Traumatic Encephalopathy in Players of American Football. JAMA 2017; 318: 360–370.

Mudher A, Colin M, Dujardin S, Medina M, Dewachter I, Alavi Naini SM, et al. What is the evidence that tau pathology spreads through prion-like propagation? Acta Neuropathol. Commun. 2017; 5: 99.

Narasimhan S, Guo JL, Changolkar L, Stieber A, McBride JD, Silva LV, et al. Pathological tau strains from human brains recapitulate the diversity of tauopathies in non-transgenic mouse brain. J. Neurosci. 2017; 37: 11406-11423.

Ojo JO, Mouzon B, Algamal M, Leary P, Lynch C, Abdullah L, et al. Chronic Repetitive Mild Traumatic Brain Injury Results in Reduced Cerebral Blood Flow, Axonal Injury, Gliosis, and Increased T-Tau and Tau Oligomers. J Neuropathol Exp Neurol 2016; 75: 636–55.

Paxinos G, Franklin KBJ. The Mouse Brain in Stereotaxic Coordinates. San Diego, CA, USA: Academic Press; 2004.

Petry FR, Pelletier J, Bretteville A, Morin F, Calon F, Hébert SS, et al. Specificity of anti-tau antibodies when analyzing mice models of Alzheimer's disease: problems and solutions. PloS One 2014; 9: e94251.

Pischiutta F, Micotti E, Hay JR, Marongiu I, Sammali E, Tolomeo D, et al. Single severe traumatic brain injury produces progressive pathology with ongoing contralateral white matter damage one year after injury. Exp. Neurol. 2018; 300: 167–178.

Prusiner SB. Novel proteinaceous infectious particles cause scrapie. Science 1982; 216: 136–44.

Prusiner SB. Cell biology. A unifying role for prions in neurodegenerative diseases. Science 2012; 336: 1511–1513.

Sanders DW, Kaufman SK, DeVos SL, Sharma AM, Mirbaha H, Li A, et al. Distinct tau prion strains propagate in cells and mice and define different tauopathies. Neuron 2014; 82: 1271–88.

Sekino Y, Koganezawa N, Mizui T, Shirao T. Role of Drebrin in Synaptic Plasticity. In: Drebrin. Springer, Tokyo; 2017. p. 183–201.

Senatore A, Colleoni S, Verderio C, Restelli E, Morini R, Condliffe SB, et al. Mutant PrP

suppresses glutamatergic neurotransmission in cerebellar granule neurons by impairing membrane delivery of VGCC alpha(2)delta-1 subunit. Neuron 2012; 74: 300–13.

Smith DH, Soares HD, Pierce JS, Perlman KG, Saatman KE, Meaney DF, et al. A model of parasagittal controlled cortical impact in the mouse: cognitive and histopathologic effects. J. Neurotrauma 1995; 12: 169–178.

Tran H. T., LaFerla FM, Holtzman DM, Brody DL. Controlled cortical impact traumatic brain injury in 3xTg-AD mice causes acute intra-axonal amyloid-beta accumulation and independently accelerates the development of tau abnormalities. J Neurosci 2011; 31: 9513–25.

Tran Hien T., Sanchez L, Esparza TJ, Brody DL. Distinct temporal and anatomical distributions of amyloid-β and tau abnormalities following controlled cortical impact in transgenic mice. PloS One 2011; 6: e25475.

Woerman AL, Aoyagi A, Patel S, Kazmi SA, Lobach I, Grinberg LT, et al. Tau prions from Alzheimer's disease and chronic traumatic encephalopathy patients propagate in cultured cells. Proc. Natl. Acad. Sci. 2016; 113: E8187–E8196.

Yoshiyama Y, Uryu K, Higuchi M, Longhi L, Hoover R, Fujimoto S, et al. Enhanced neurofibrillary tangle formation, cerebral atrophy, and cognitive deficits induced by repetitive mild brain injury in a transgenic tauopathy mouse model. J Neurotrauma 2005; 22: 1134–41.

Zanier ER, Marchesi F, Ortolano F, Perego C, Arabian M, Zoerle T, et al. Fractalkine Receptor Deficiency Is Associated with Early Protection but Late Worsening of Outcome following Brain Trauma in Mice. J. Neurotrauma 2016; 33: 1060–1072.

Figure Legends

Figure 1. Tau pathology in survivors of a single moderate or severe TBI. (**A**) Typically, controls showed sparse P-tau immunoreactive neurofibrillary tangles and neurites localized to the entorhinal cortex (**i**; 59-year-old male). In contrast, patients surviving a year or more from single moderate or severe TBI showed more extensive neurofibrillary, neuritic and glial P-tau immunoreactive profiles, with occasional clusters around cortical vessels in a 'CTE-like' manner (**ii**; 59-year-old male 17 year survival from single severe TBI), and extending beyond the entorhinal cortex to involve wider grey matter regions including the hippocampus (**iii**; 87-year-old male 5 year survival from single severe TBI). (**B**) While the proportion of patients in TBI and controls with tau pathologies was similar, following TBI the extent and distribution of pathology was considerably greater. Thus, using a semi-quantitative scheme to score tau distribution, while all but 4 controls showed no or only localized tau pathology (Score 0 or 1), in a majority of TBI cases (9 of 15) P-tau pathology was widespread (Score 2 or 3; p=0.0035; ChiSq). All sections stained for PHF-1. Scale bar: 100 μm.

Figure 2. Evidence of tau pathology in mouse TBI. AT8 immunostaining and quantification of the AT8-positive area in the ipsilateral and contralateral cortex of sham and TBI mice at 3 and 12 months post injury. (**A, B**) AT8 immunoreactivity is detected in the ipsilateral (ipsi) pericontusional cortical area in 2 out of 4 mice at 3 months post TBI, and in all mice at 12 months. (**C, D**) In the contralateral cortex AT8 immunoreactivity is detected only after 12 months post TBI. Data are mean ± SEM; n = 4-5; *p < 0.05; **p < 0.01 by one-way ANOVA, Tukey post-hoc test. Scale bar: 100 μm (B, D).

Figure 3. Widespread tau pathology in mice 12 months post TBI. Examples of tau immunostaining with the AT180 (**A, F**), PHF1 (**B**), and AT8 (**C-E, G, H**) antibodies in the cerebral cortex (A, B), CA1 (C) and CA3 (D) fields of the hippocampus, and in the zona incerta (E, F). Examples of clusters of small to medium sized, rounded, 'grain-like' profiles, in the zona incerta (G), and granular profiles along a cortical vessel (H; arrows). Scale bars: 20 μm (A-D, G); 10 μm (E, F); 50 μm (H).

Figure 4. Inoculation of contused tissues induces memory deficits in wild-type mice. (**A**) Groups of mice used in the inoculation studies. C57BL/6J male mice were either left untreated (white) or inoculated bilaterally into the hippocampus and overlaying cerebral cortex with 10% brain homogenates from sham mice (grey) or from the contused (TBI_{ipsi}, indigo) or contralateral (TBI_{contra}, magenta) hemisphere at 12 months post TBI. (**B, C**) Recognition memory was investigated by the novel object recognition (NOR) test at 8 (B) and 12 (C) months after inoculation. Performance in the NOR task was expressed as discrimination index (the higher the discrimination index the better the performance). **(D, E)** Locomotor activity was

similar in naïve, sham and TBI inoculated mice at 8 (D) and 12 (E) months after inoculation. Data are mean ± SEM; *p < 0.05, vs. naive; $^{\#}$p < 0.05 vs. sham by one-way ANOVA, Tukey post-hoc test.

Figure 5. Memory deficits are already detected at four months post-inoculation. (**A**) Scheme of the groups of mice used in the inoculation studies. C57BL/6J male mice were either left untreated (white) or inoculated bilaterally into the hippocampus and overlaying cerebral cortex with 10% brain homogenates from sham (grey) or TBI (contused hemisphere, indigo) mice 12 months post-injury. (**B, C**) Recognition memory was investigated by novel object recognition (NOR) test at 4 (B) and 8 (C) months after inoculation. Histograms indicate the discrimination index (the higher the discrimination index the better the performance). (**D, E**) Locomotor activity was similar in sham and TBI inoculated mice at 4 (D) and 8 (E) months after inoculation. Data are mean ± SEM, n = 11-14. ***p < 0.001, **p < 0.01 vs. naive; $^{\#\#}$p < 0.01 vs. sham; by one-way ANOVA, Tukey post-hoc test.

Figure 6. Synaptic alterations in the hippocampus of TBI inoculated mice. (**A, B**) Representative images of immunofluorescence staining and quantitative analysis of presynaptic (VGLUT-1; A) and postsynaptic (drebrin; B) markers in the hippocampus of the inoculated mice at 12 months post inoculation. Data are mean ± SEM; n = 5-6; *p < 0.05; **p < 0.01 by unpaired t-test. Scale bar: 10 μm. (**C**) Representative electron micrographs of stratum oriens synapses, and quantification of the thickness and area of the postsynaptic density (PSD) in sham and TBI inoculated mice. Data are mean ± SEM; n = 3. *p<0.05 by unpaired t-test. Scale bar: 100 nm.

Figure 7. Evidence of tau pathology in mice inoculated with TBI homogenates. Quantification of the percent area covered by AT8 staining in the cortex (**A-C**), hippocampus (**D-F**), thalamus (**G-I**), and cerebellum (**J-L**). Data are mean ± SEM; n = 3-6; *p < 0.05; **p < 0.01 by unpaired t-test. Scale bars: 100 μm (D-I) and 200 μm (K, L).

Figure 8. Widespread tau pathology in mice inoculated with TBI homogenates. Representative micrographs of tau immunostaining in the brains of mice inoculated with sham (**A**) and TBI (**B-K**) homogenates. Examples of immunostaining with AT8 (A-C, F-H, K), PHF1 (D, I, J) and conformation-dependent antibody MC1 (E) in the hippocampus (A, B, E, F), cerebral cortex (C, D), thalamus (G, H, I) and cerebellum (J, K). CA1 and CA3, fields of the hippocampus; LMol, stratum lacunosum molecolare; M, molecular layer; PC, Purkinje cell layer; G, granule cell layer. Scale bars: 200 μm (A, B); 50 μm (C); 20 μm (E, F, G, J, K); 10 μm (D, H); 5 μm (I).

Supplementary Material

Supplementary Table

	TBI (n=15)	Controls (n=15)
Median age (range)	60 years (19-89)	60 years (20-92)
Males	12	11
Median TBI survival (range)	5 years (1-18)	NA
Mean pm delay (range)	52 hours (19 h – 5 days)	39 hours (12 h – 6 days)
Cause of TBI		NA
Road traffic accident	5	
Fall	5	
Assault	3	
Not known	2	
Cause of death		
Respiratory	6	8
Cardiovascular disease	4	1
Gastrointestinal disease	2	2
Trauma	2	0
Seizure	1	0
Malignancy	0	2
Sepsis	0	2

Supplementary Table 1. Demographic and clinical data for TBI and control subjects.

Legend: PM = post mortem; NA = not applicable. Controls had no known history of TBI.

Supplementary Figures

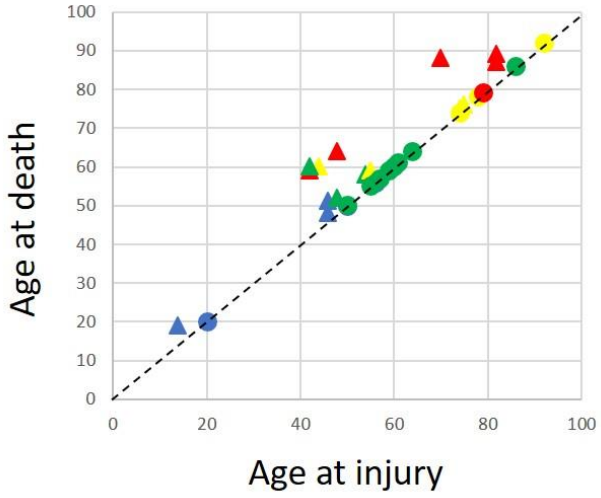

Supplementary Figure 1: Extent of tau pathology against age and survival interval in late TBI cases and controls. *(Key to plot: circles, controls; triangles, late TBI cases; blue, tau score 0; green, tau score 1; yellow, tau score 2; red, tau score 3).* Higher score tau pathology (score 2 or 3) was broadly associated with older age in both controls and in late TBI patients, though with this level of pathology present from a younger age in TBI survivors (59 and above) compared to controls (74 and older). No clear association between survival interval and extent of tau pathology was present. The x-axis represents the age at injury, the y-axis age at death. For controls these figures are the same, with this intersection marked by the dotted line. Vertical deviations from that line in late TBI cases are equivalent to survival interval.

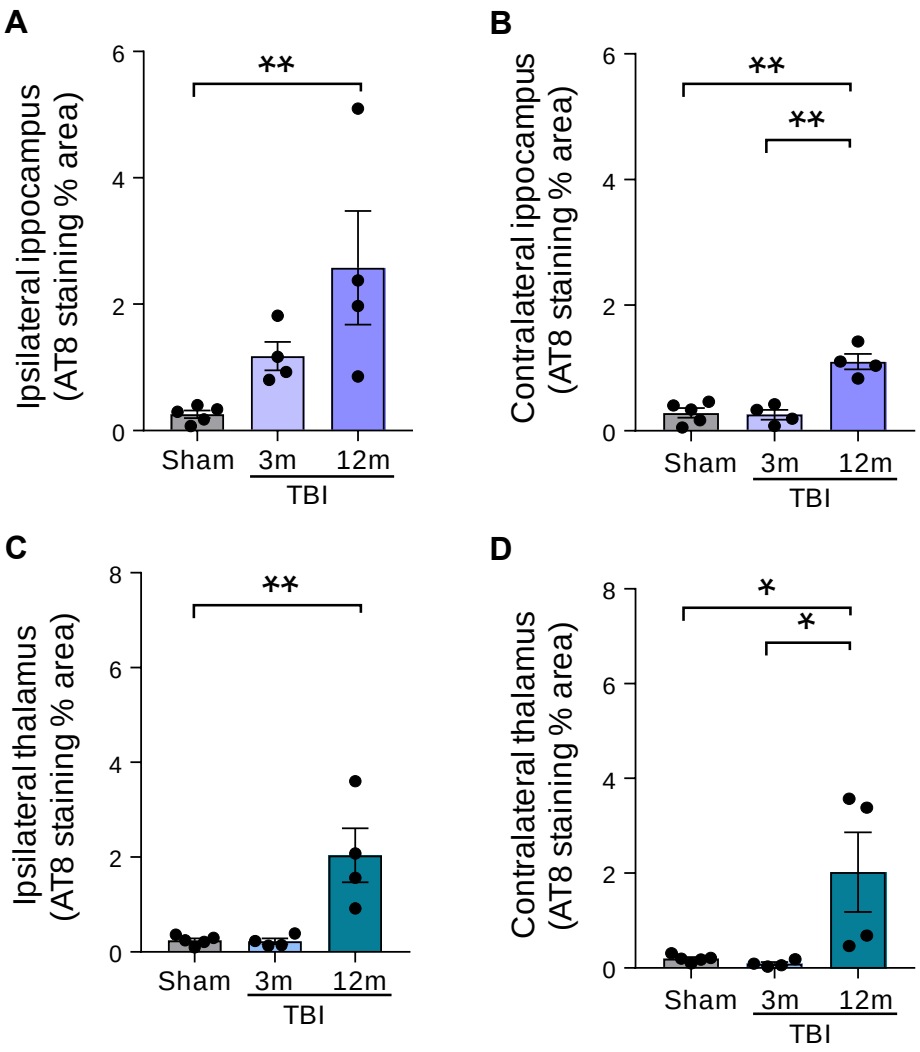

Supplementary Figure 2. Evidence of tau pathology in hippocampus and thalamus in TBI mice. Quantification of the AT8-positive area in the ipsilateral and contralateral hippocampus (**A, B**) and thalamus (**C, D**) of sham and TBI mice at 3 and 12 months post injury. Data are mean ± SEM; n = 4-5; *p < 0.05; **p < 0.01 by one-way ANOVA, Tukey post-hoc test.

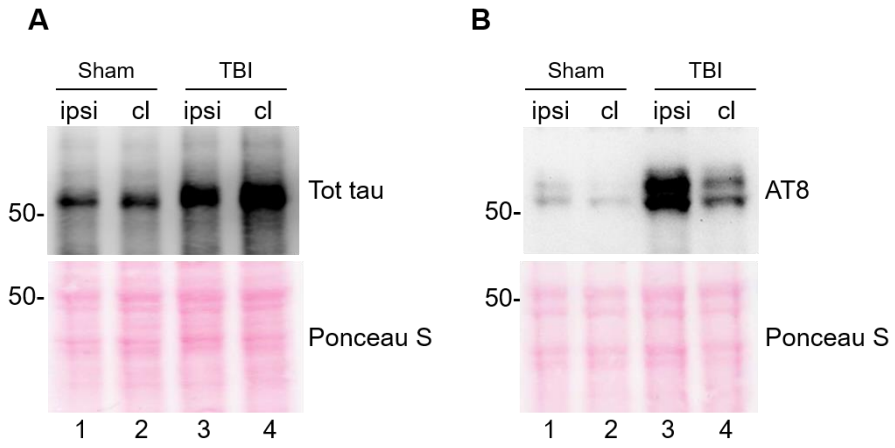

Supplementary Figure 3. Example of Western blot analysis of tau in sham and TBI mice. Western blot analysis of the pericontusional (ipsi) and corresponding contralateral (cl) area with anti-total tau (**A**) and AT8 (**B**) antibodies at 12 months post TBI or sham injury. Ponceau S staining of the blots (bottom panels) show similar amounts of total proteins.

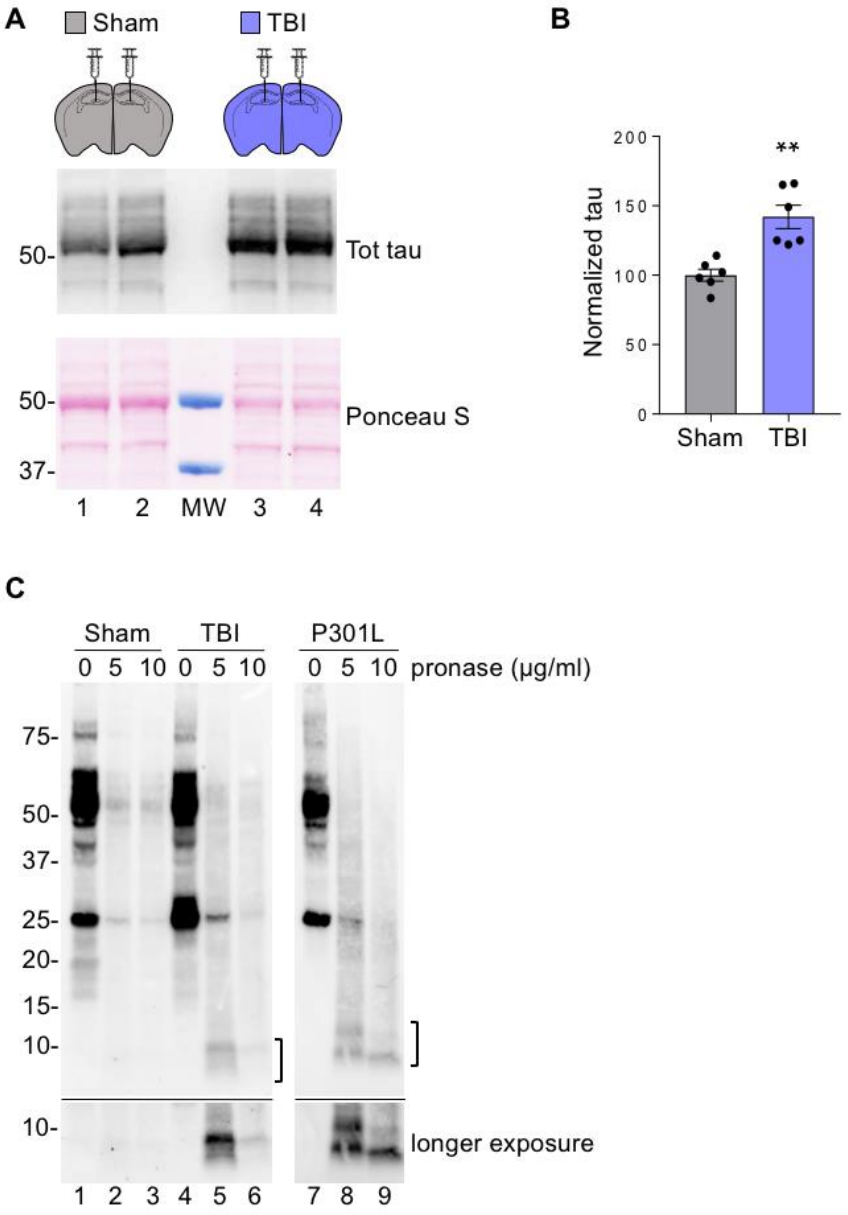

Supplementary Figure 4. Detergent-insoluble and protease-resistant tau in mice inoculated with TBI homogenates. Detergent-insoluble tau in dissected thalami of mice inoculated with (**A**) sham or TBI brain homogenates, was analyzed by Western blot using an anti-total tau antibody. The amount of insoluble tau was quantified by densitometric analysis of Western blots, normalized for the total amount of proteins determined by Ponceau S staining of the blot (bottom panel), and expressed as a percentage of the amount in sham-inoculated mice (**B**). Data are mean ± SEM, n = 6. **p < 0.01 by unpaired t-test. (**C**) Triton X-100 lysates of thalami dissected from sham and TBI inoculated mice were incubated with 0-10 µg/mL pronase for 1h at 37°C, and tau was visualized by Western blot using antibody BR135. The bracket indicates the protease-resistant bands, also shown in the longer exposure. Transgenic mice overexpressing mutant tau P301L (Lewis J et al., Nature Genetics 2000), displaying tau seeding activity (de Calignon *et al.*, 2012; Liu *et al.*, 2012) were used as a positive control. Result is representative of three independent experiments.

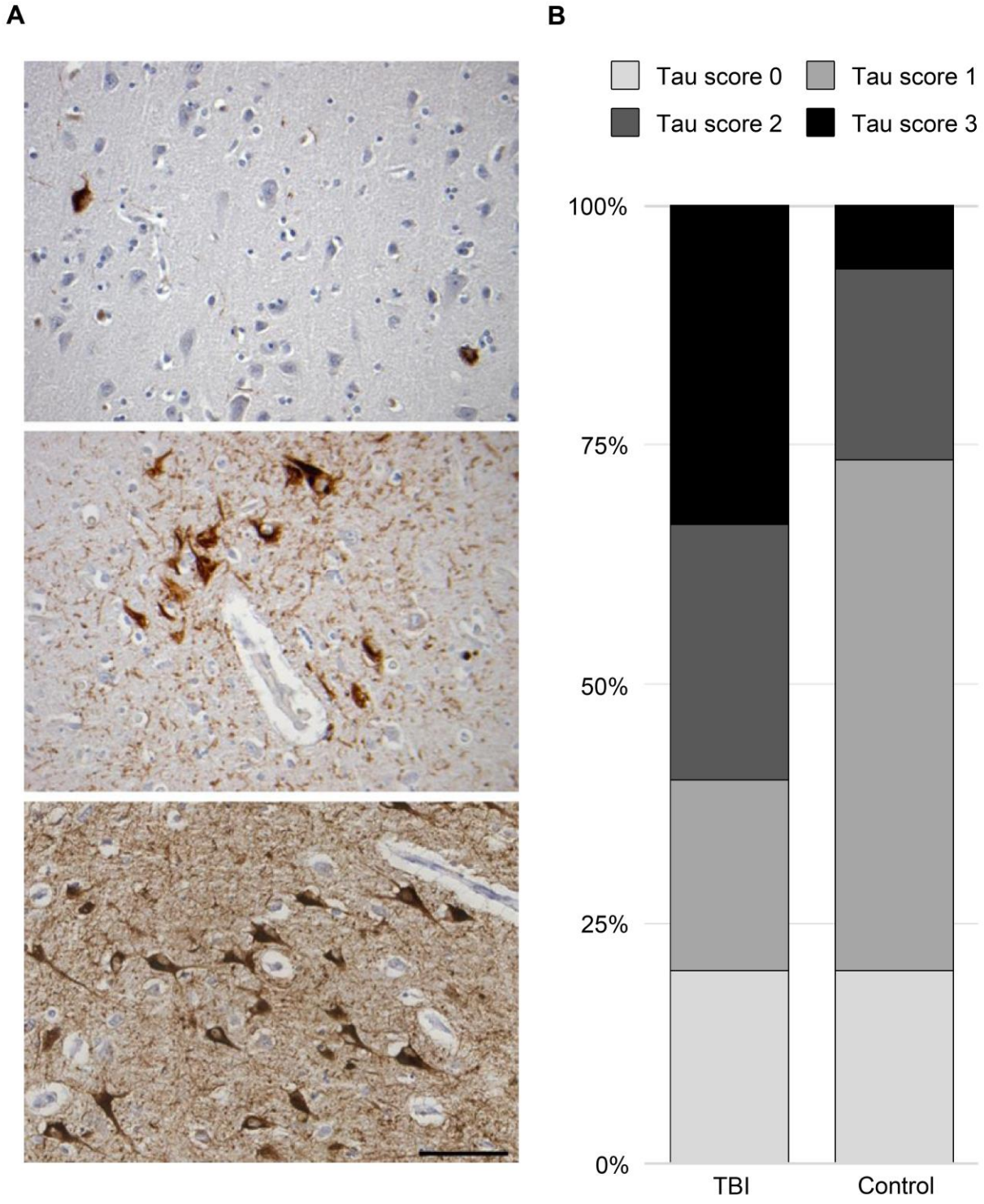
A
B
Tau score 0
Tau score 1
Tau score 2
Tau score 3
100%
75%
50%
25%
0%
TBI
Control

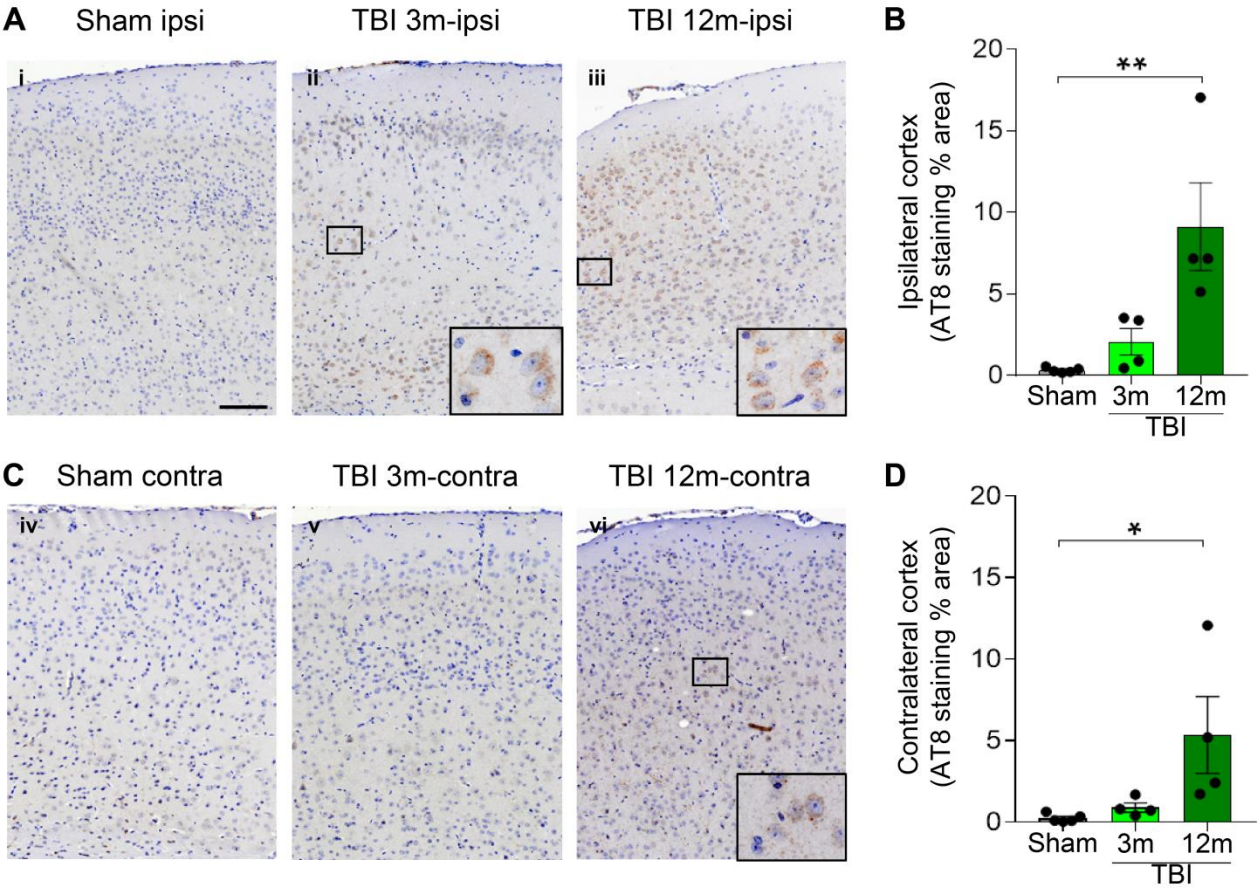
A
Sham ipsi
TBI 3m-ipsi
TBI 12m-ipsi
i
ii
iii
B
Ipsilateral cortex
(AT8 staining % area)
20
15
10
5
0
**
Sham
3m
12m
TBI
C
Sham contra
TBI 3m-contra
TBI 12m-contra
iv
v
vi
D
Contralateral cortex
(AT8 staining % area)
20
15
10
5
0
*
Sham
3m
12m
TBI

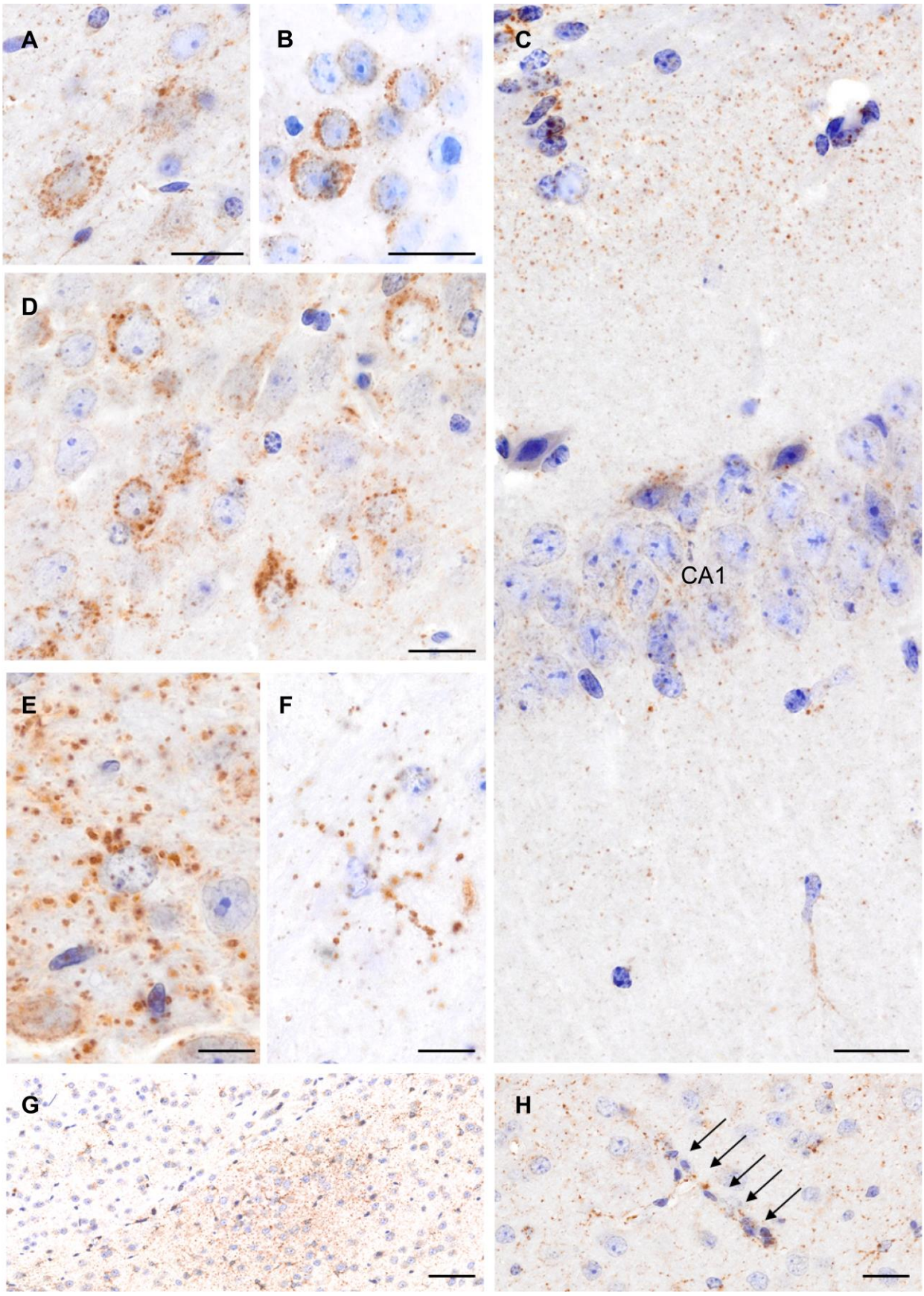
A
B
C
D
CA1
E
F
G
H

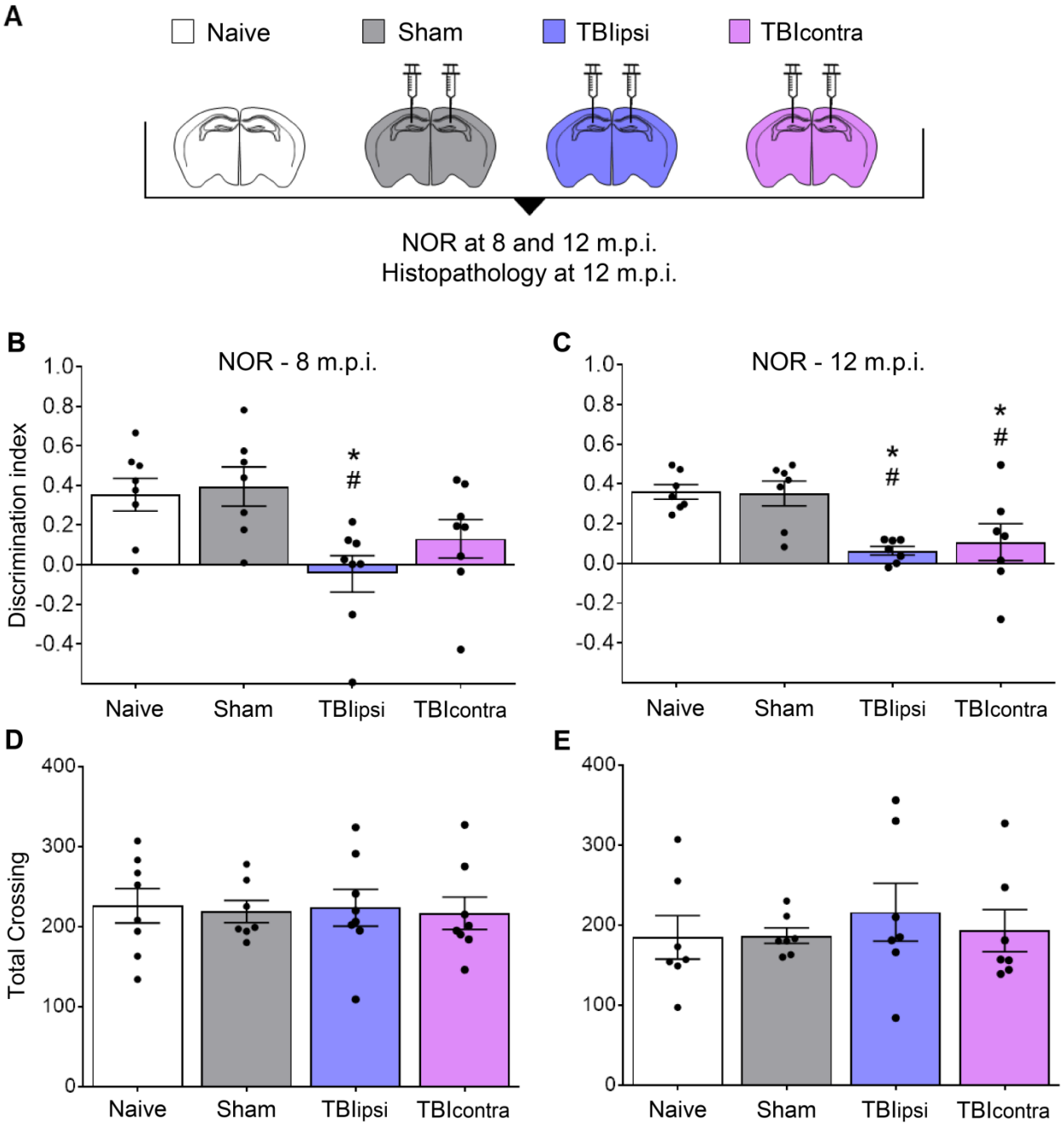
A
Naive
Sham
TBIipsi
TBIcontra
NOR at 8 and 12 m.p.i.
Histopathology at 12 m.p.i.
B
NOR - 8 m.p.i.
Discrimination index
1.0
0.8
0.6
0.4
0.2
0.0
-0.2
-0.4
*
#
Naive
Sham
TBIipsi
TBIcontra
C
NOR - 12 m.p.i.
D
Total Crossing
400
300
200
100
0
E

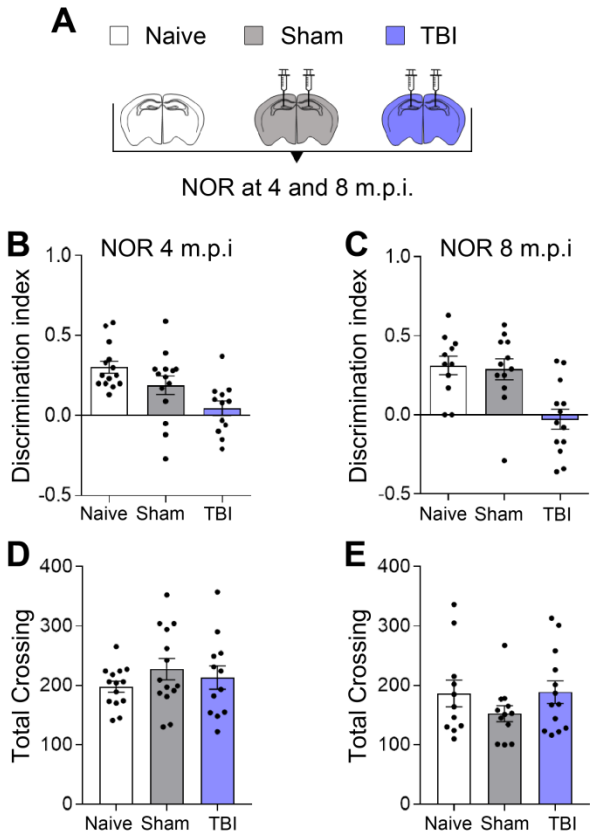
A
Naive
Sham
TBI
NOR at 4 and 8 m.p.i.
B
NOR 4 m.p.i
Discrimination index
1.0
0.5
0.0
-0.5
Naive Sham TBI
C
NOR 8 m.p.i
Discrimination index
1.0
0.5
0.0
-0.5
Naive Sham TBI
D
Total Crossing
400
300
200
100
0
Naive Sham TBI
E
Total Crossing
400
300
200
100
0
Naive Sham TBI

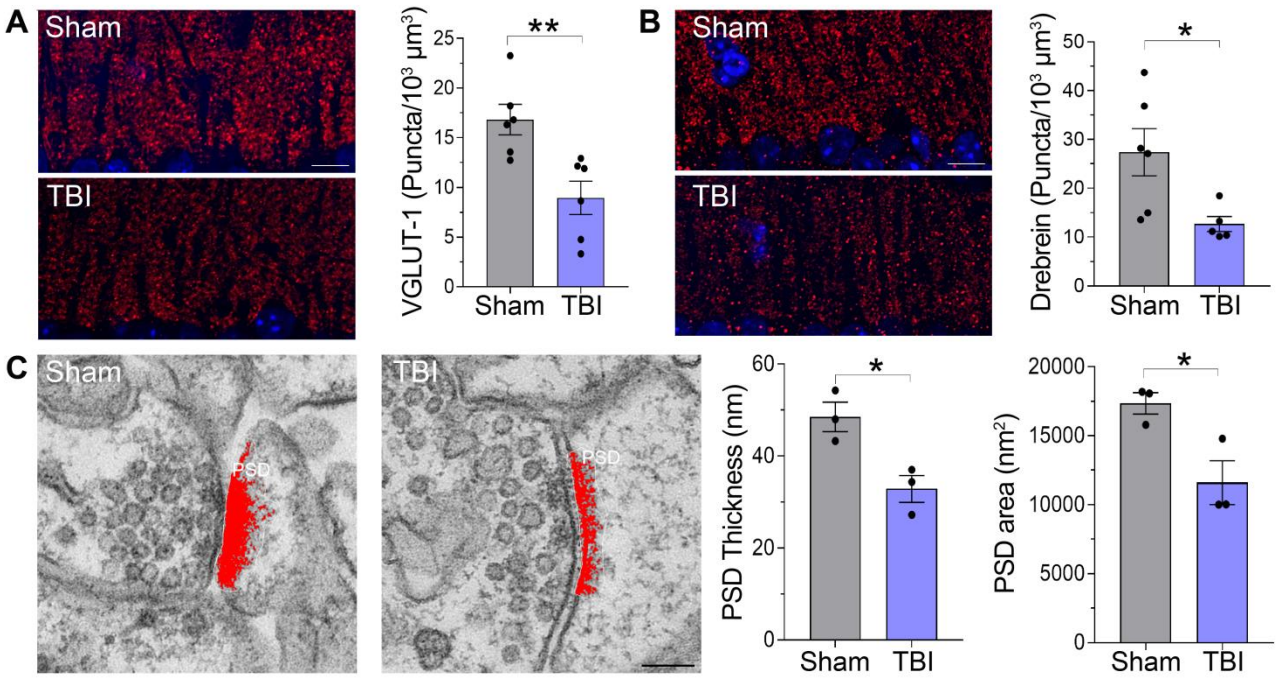
A
Sham
TBI
VGLUT-1 (Puncta/10³ µm³)
**
Sham
TBI
B
Sham
TBI
Drebrein (Puncta/10³ µm³)
*
Sham
TBI
C
Sham
PSD
TBI
PSD
PSD Thickness (nm)
*
Sham
TBI
PSD area (nm²)
*
Sham
TBI

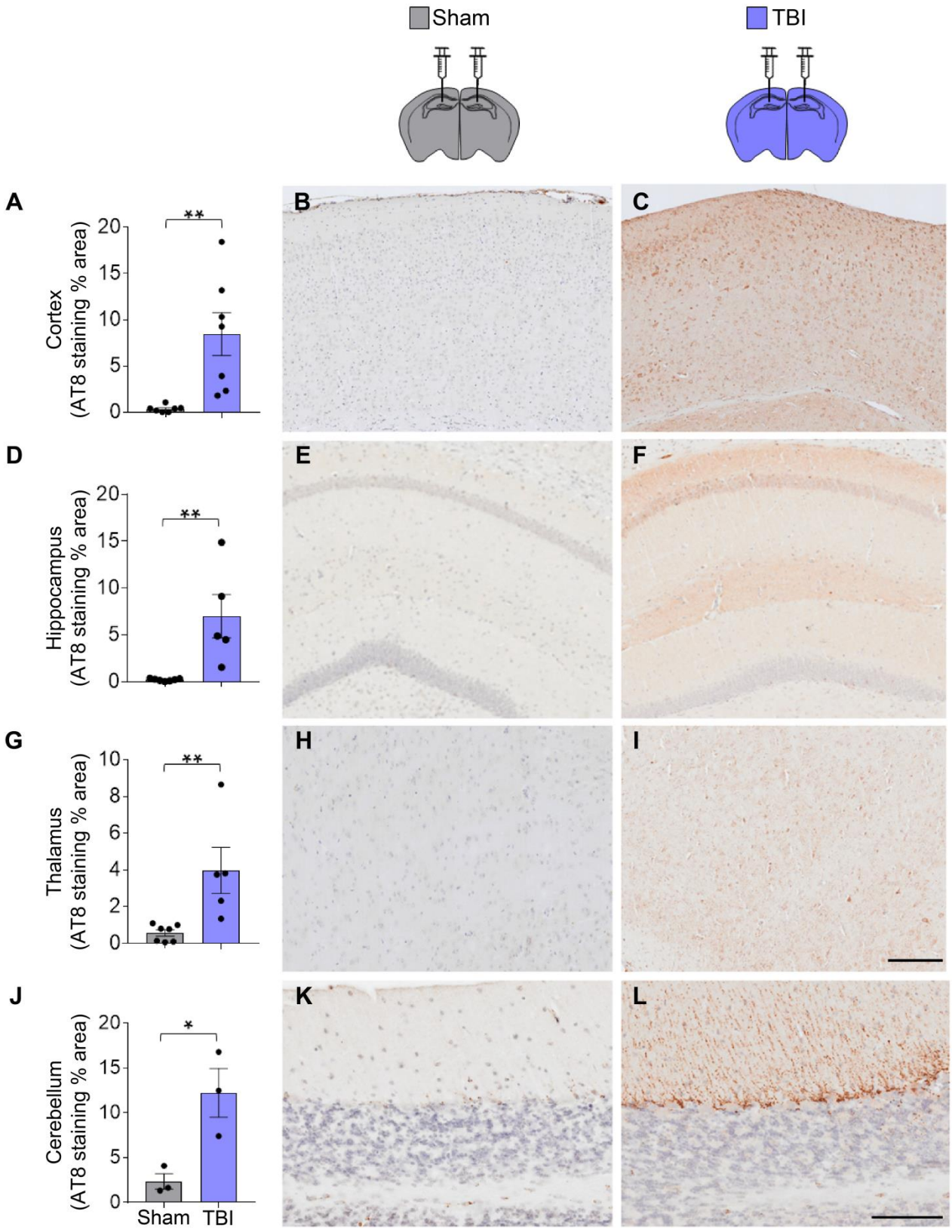
Sham
TBI
A
B
C
Cortex
(AT8 staining % area)
20
15
10
5
0
**
D
E
F
Hippocampus
(AT8 staining % area)
20
15
10
5
0
**
G
H
I
Thalamus
(AT8 staining % area)
10
8
6
4
2
0
**
J
K
L
Cerebellum
(AT8 staining % area)
20
15
10
5
0
*
Sham
TBI

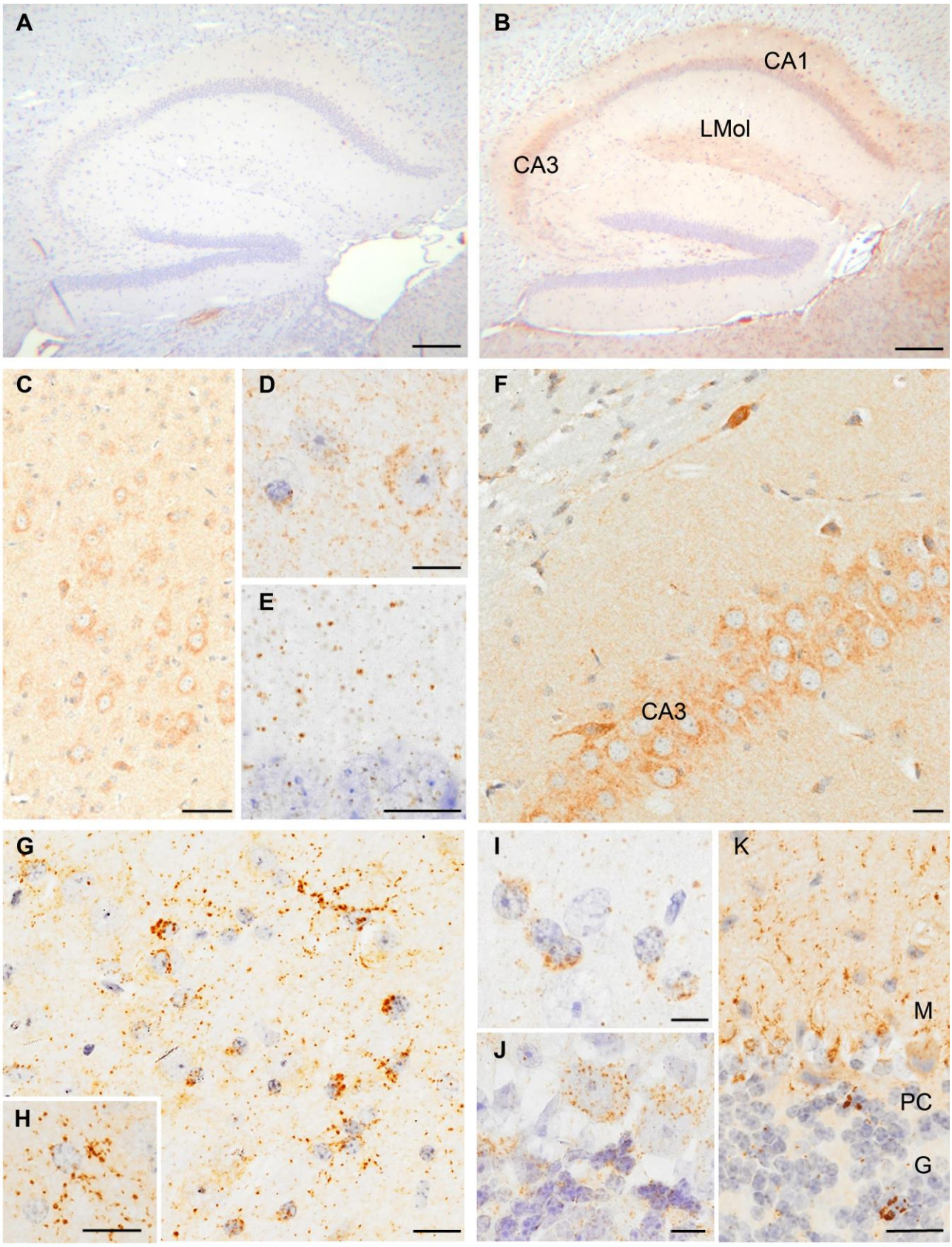
A
B
CA1
LMol
CA3
C
D
E
F
CA3
G
H
I
J
K
M
PC
G